JOURNAL OF BIOMOLECULAR STRUCTURE AND DYNAMICS
https://doi.org/10.1080/07391102.2021.1910570

The *in silico* mechanism of hVKOR interaction with acetaminophen and its metabolite, as well as N-acetyl cysteine: caution on application in COVID-19 patients

S. Ali Hashemi[a,b], Armita Kyani[c] and S. Zahra Bathaie[a]

[a]Department of Clinical Biochemistry, Faculty of Medical Sciences, Tarbiat Modares University, Tehran, Iran; [b]Department of Laboratory Sciences, Chalus Branch, Islamic Azad University, Chalous, Iran; [c]Department of Medicinal Chemistry, College of Pharmacy, University of Michigan, Ann Arbor, MI, USA

Communicated by Ramaswamy H. Sarma

ABSTRACT

Acetaminophen and N-acetyl cysteine (NAC) are being used as supportive care in patients suffering from coronavirus disease 2019 (COVID-19). The coagulopathy and cerebral hemorrhage have been recently reported in these patients. Prolonged acetaminophen use increases the international normalized ratio (INR) and the risk of bleeding among patients taking anti-coagulants. Inhibition of vitamin K epoxide reductase (VKOR) by acetaminophen and NAC in chronic applications has been reported, however, detailed knowledge of the molecular mechanism and binding sites are not clear. Herein, we built the homology model of human VKOR (hVKOR) using ITASSER server, confirmed, and applied it for docking analysis of its interaction with acetaminophen and its metabolite, N-acetyl-p-benzoquinone imine (NAPQI), and NAC. We also calculated the lipophilicity and predicted the blood-brain-barrier (BBB) permeation of NAPQI by Swiss ADME. Our analysis showed that NAPQI and NAC, but not acetaminophen, bind strongly to the similar sites in hVKOR via both hydrogen and van der Waals bonding; particularly with Cys135. Thus, it interrupted the vitamin K reducing electron transfer pathway. Further, molecular dynamic (MD) simulation study revealed that the interactions of the ligands with hVKOR are stable. In conclusion, our analysis shed a light on the molecular mechanism of acetaminophen-induced coagulopathy previously reported in some clinical cases with chronic acetaminophen use. Furthermore, considering the anti-coagulopathy of NAPQI and NAC but not acetaminophen, the BBB permeation potency of these agents, and the risk of coagulopathy in COVID-19, we suggest a regular prothrombin time (PT) and INR monitoring of these patients taking acetaminophen and/or NAC.

ARTICLE HISTORY
Received 15 August 2020
Accepted 25 March 2021

KEYWORDS
NAPQI; NAC; INR; docking analysis; molecular dynamics simulation; coagulopathy

Introduction

Acetaminophen is a commonly used analgesic and antipyretic drug, which recently is recommended as a supportive care for the patients with coronavirus disease 2019 (COVID-19) or SARS-CoV-2 (CDC, 2020; Gupta & Misra, 2020; Noah Berland et al., 2020). The previous reports indicated that pain and fever are among the most common COVID-19 symptoms (Salehi et al., 2020; Song et al., 2020). In addition, patients with COVID-19 also suffer from coagulopathy and prolonged prothrombin time (Chen et al., 2020; Wang et al., 2020), as well as increased D-dimers (Tang et al., 2020). The pooled analysis also revealed that lower platelet count was significantly correlated with the more severe COVID-19 (Lippi et al., 2020). The new line of evidences showed a poor prognostic feature in COVID-19 patients with coagulopathy (Lippi et al., 2020), which is even accompanied by cerebral hemorrhage.

On the other hand, previous case reports have shown that acetaminophen application for a long period of time may lead to increased international normalized ratio (INR) and the risk of bleeding among patients taking anticoagulants (Andrews, 2002; Boeijinga et al., 1982; Mahe et al., 2006; Mackerell et al., 1998; Meng et al., 2011; Parra et al., 2007; Rubin et al., 1984). Inhibition of the activity of the enzymes involved in vitamin K cycle by the acetaminophen toxic metabolite, N-acetyl-p-benzoquinone imine (NAPQI), has been proposed as a mechanism to be responsible for augmenting of warfarin anticoagulating effects (Thijssen et al., 2004). The authors reported that NAPQI and N-acetyl cysteine (NAC), but not acetaminophen inhibited the vitamin K cycle enzymes, particularly vitamin K epoxide reductase (VKOR) (Thijssen et al., 2004). NAC is an intracellular glutathione (GSH) restoring agent (Poole, 2015), which has been shown to be protective in acute pulmonary damage (Akdur et al., 2008) and against some other toxic agents (Nouri et al., 2017; Shadnia et al., 2007; Shalby et al., 2011). Recently, NAC has been used as supportive care in patients with COVID-19 (Kouhpayeh et al., 2020; Liu et al., 2020). As an emerging and urgent strategy for fighting against COVID-19, computational analysis has been used to investigate the interaction between different drugs and the virus proteins (Bhardwaj et al., 2020; de Lima Menezes & da Silva, 2020;

CONTACT S. Zahra Bathaie zbatha2000@yahoo.com; bathai_z@modares.ac.ir Department of Clinical Biochemistry, Faculty of Medical Sciences, Tarbiat Modares University, Tehran 14155-331, Iran.

Mahmud et al., 2020; Rout et al., 2020). To our knowledge, detailed data on the molecular mechanism of the acetaminophen induced hemorrhage is lacking in the literature. In addition, side effects of acetaminophen or NAC application in COVID-19 patients have not reported, yet. In the present study, we applied the computational analyses to provide some virtual evidences on the molecular mechanism of acetaminophen-/NAC-induced coagulopathy and the possibility of cerebral hemorrhage in COVID-19 patients using acetaminophen or NAC as a supportive care.

Methods

Data banks and servers

RSCB Protein Data Bank (PDB), (https://www.rcsb.org/), was used to obtain the x-ray crystal structure of a bacterial homolog of VKOR enzyme (PDB ID: 3KP9) (Li et al., 2010). The PubChem data bank for chemical structures was used to obtain the structures of acetaminophen, NAPQI and N-acetylcysteine (NAC). National center for biotechnology (NCBI), (https://www.ncbi.nlm.nih.gov/), was used for protein alignment. Iterative Threading ASSEmbly Refinement (I-TASSER) server (https://zhanglab.ccmb.med.umich.edu/I-TASSER/) used for homology modeling of hVKOR. Swiss ADME server (http://www.swissadme.ch/) was used to investigate the physicochemical descriptors of the ligands such as lipophilicity, water insolubility, and BBB permeability.

Softwares

AutoDock Vina (version 1.1.2) (Trott & Olson, 2010) was used for performing docking analysis. Auto Dock Tools (ADT) was applied to prepare ligands and protein structures for docking. MOE (version 2015.10) was used to visualize the interaction of ligands with protein in ribbon diagram. MOE was also used to determine the amino acid residues contributing in the ligand-protein interactions and also determining the kind of interactions. GROMACS 2020.4 software.

(Berendsen et al., 1995) was used for molecular dynamics simulation of the ligand-hVKOR complexes.

Protein sequence alignment

The protein BLAST tool from NCBI (https://www.ncbi.nlm.nih.gov) was applied for aligning the protein sequences of hVKOR (accession number: AAS01052.1) and *Synechococcus sp* (accession number: WP 011433847.1).

Molecular modeling of hVKORC1 homology modeling

The I-TASSER automated modeling server (https://zhanglab.ccmb.med.umich.edu/I-TASSER) was used to construct the hVKORC1 homology models based on an available 3.6 Å resolution of prokaryotic (*Synechococcus sp*) x-ray crystallographic structure (PDB ID: 3KP9). Five models were generated. The best model with the highest calculated C-score and estimated TM-score was selected. The backbone comparison between the model and template structures was conducted through Pymol alignment function.

Docking protocol

The mechanism of interactions and binding sites of ligands including; NAPQI, N-acetyl cysteine (NAC) and acetaminophen with the homology model of VKOR were determined by docking protocol used in our previous studies (Hashemi et al., 2020a, 2020b; Hashemi, Karami, & Bathaie 2020). Briefly, PDB files of the ligands (NAPQI, NAC, or acetaminophen) were imported into ADT. Polar hydrogens were added, and Gasteiger charges were computed. Rigid roots, rotatable bands and torsion tree were determined as requested by the software. Then, the protein was prepared for docking process by importing the PDB file of homology-based model into ADT. Then, Kollman charge was added. After preparation, ligands and protein were saved separately as PDBQT format. The grid box with map of $100 \times 100 \times 100$ points and grid-point spacing of 0.375 Å was determined and used for docking of all ligands. Docking command was issued, while exhaustiveness was 100. After computation, 9 conformers of the ligand-protein interaction were proposed for each ligand. The conformers were scored in order of the binding energy strength (kcal/mol). The conformers were surveyed and visualized by Pymol and MOE and the amino acid residues and the binding forces in the ligand-protein interaction were determined by MOE. In order to compare the binding sites of and NAPQI and NAC with acetaminophen in VKOR structure, the ligand-protein complexes were overlaid and the enzyme structure was removed.

To examine the validity of docking analysis, we extracted the quinone from the VKOR X-ray crystal structure and docked it with the quinone-free structure and compared the binding site of the best conformer with the original binding site.

Molecular dynamics simulation of ligand-VKOR complexes

Ligand-hVKOR complexes with the lowest binding energy were selected for molecular dynamics (MD) simulation. CHARMM36 force field (Brooks et al., 1983; Huang & Mackerell, 2013; MacKerell et al., 1998) was used to construct the topology.

The ligand parameters were generated using CGenFF online server (https://cgenff.umaryland.edu).

The ligand-protein complex was solvated using a simple point charge (Berendsen et al., 1981) water box under periodic boundary conditions using 1.0 nm distance from the protein to the box faces. The system was then neutralized by Cl^- counter ions for three complexes.

Energy minimization was done for 1,000 steps by the steepest descent method (Attouch & Cominetti, 1996). For the sake of flowing energy minimization, the systems were equilibrated under constant number of particles, volume, and temperature conditions for 100 ps at 300 K, followed by 100 ps under constant number of particles, pressure, and temperature conditions. All the covalent bonds with hydrogen atoms were constrained using the Linear Constraint

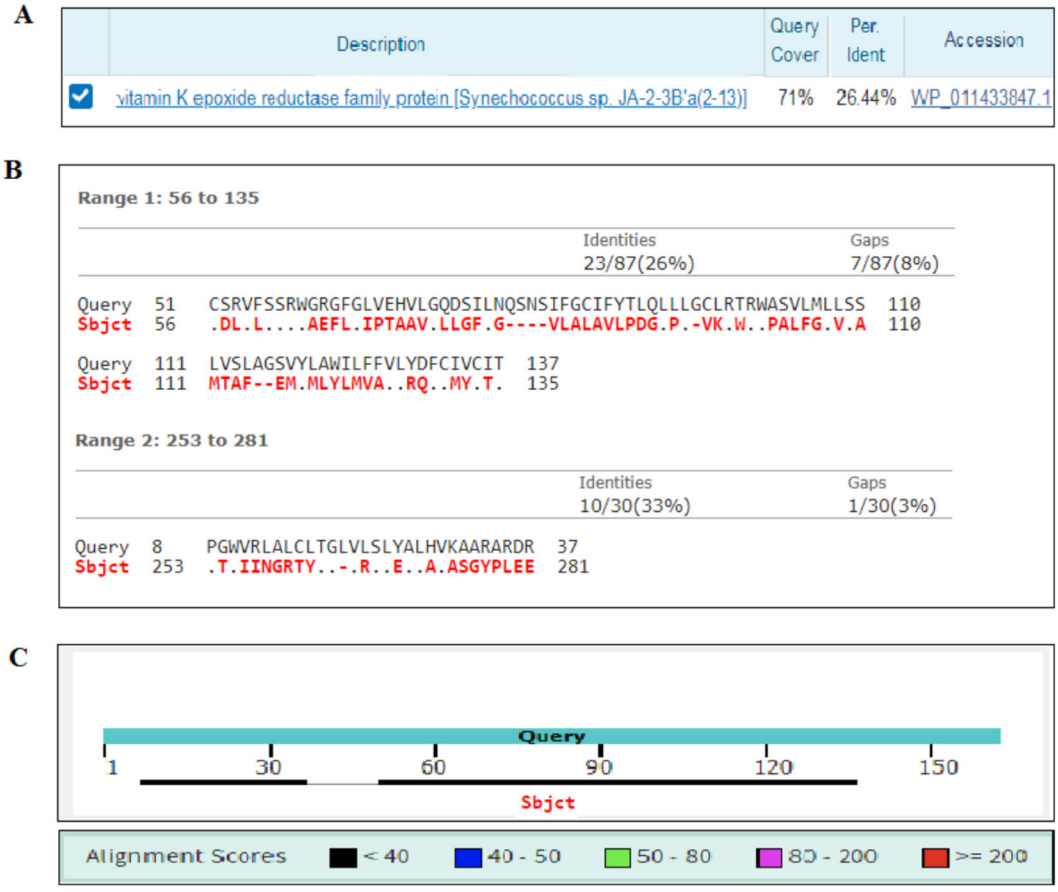

Figure 1. Sequence alignment of human and *Synechococcus sp* VKOR proteins. (A) The percentage of protein sequence alignment coverage between the query and subject. (B) The percentages of the identity and gap sites in the subject. (C) Alignment score and distribution of aligned sequences of the subject regarding to the query. Subject: human hVKOR with accession number: AAS01052.1; query: *Synechococcus sp* with accession number: WP 011433847.1.

Solver algorithm. The electrostatic interactions were treated using the Particle Mesh Ewald method (Essmann et al., 1995). Finally, MD simulation was performed for 20 ns to check the stability of the ligand-protein complexes.

The potential of each trajectory produced after MD simulations were analyzed using g_rms and g_rmsf, of GROMACS utilities, (Van Der Spoel et al., 2005) and the root mean square deviation (RMSD) and root mean square fluctuation (RMSF) were obtained.

Physicochemical and pharmacokinetic characteristics of acetaminophen and NAPQI

To compare the possibility of NAPQI and acetaminophen permeation into the BBB, the Swiss ADME server was used in our study. Some physicochemical properties of both agents were calculated and the results were plotted on a radar diagram. In addition, the BOILED-Egg plot was prepared to estimate the possibility of permeation into BBB.

Results

The homology of VKOR protein sequence of human and Synechococcus sp

Figure 1 shows the results of amino acid sequence alignment of the hVKOR and *Synechococcus sp*, using the NCBI protein BLAST tool. Figure 1(A) indicates that 71% of the bacterial VKOR amino acid residues were covered in the alignment and only 26% identical residues were observed between the subject (hVKOR; accession number: AAS01052.1) and the query (*Synechococcus sp*; accession number: WP 011433847.1). Figure 1(B) shows the distribution of identities, aligned residues and gap areas by the query and the subject. Figure 1(C) graphically visualizes the distribution of the aligned areas in the subject sequence. As the figures indicate the alignment earned the minimum score.

The quality of hVKOR homology model

Table 1 shows the characteristics of the homology model built by ITASSER for hVKOR. This table shows that bacterial X-ray crystal structure (PDB ID: 3KP9) used as the best template for the multi-threading program. The normalized Z-score for this alignment was 6.95. The predicted homology model with highest rank showed a confidence (C)-score of 0.43 and the template modeling (TM)-score of 0.77. As Table 1 indicates, structural alignment of the homology model with the 3KP9 structure showed a root mean- square deviation (RMSD); 1 Å (i.e. 0.96 Å), TM-score; 0.813, and sequence coverage of 0.841. Figure 2 shows the homology of hVKOR with bacterial one, regarding the composition of secondary structures and localization in cell membrane. The figure shows that the most part of the 4-transmembrane structure

Table 1. Analyses and quality parameters of the hVKOR homology modeling.

Analysis	Parameter	Result
Structure threading[a]	Normalized Z-score of the template	6.95
	PDB ID of the best template	3kp9
Model prediction[b]	C-score of the top model	0.43
	TM-score	0.77 ± 0.10
	RMSD (Å)	4.1 ± 2.7
Structural alignment of the selected model[c]	TM-score	0.813
	RMSD (Å)	0.96
	Structural alignment coverage	0.841
	PDB ID of the best analogue	3kp9A

[a]Conducted by LOMETS threading program.
[b]Conducted by SPICKER program.
[c]Conducted by TM-align structural alignment program.

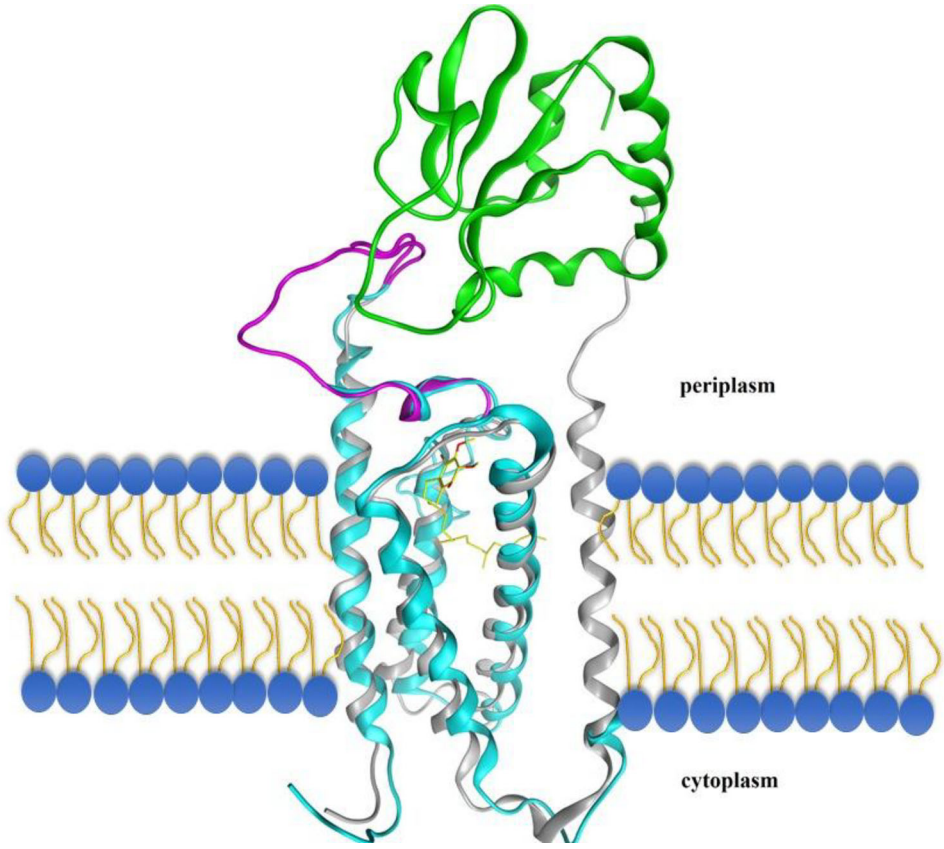

Figure 2. Structural alignment of hVKOR homology-based model protein and *Synechococcus sp* VKOR protein. The cyan and gray color ribbons show the hVKOR and *Synechococcus sp* VKOR proteins, respectively. TMs 1–4 that are homologous to the mammalian VKOR are overlapped. The loop containing the 1/2-segment and 1/2-helix, is shown in magnetic color. Quinone is shown as a yellow stick within the molecule. The membrane phospholipids are shown as yellow-blue shapes. Trx-Like domain is shown in green.

of the hVKOR is located in the cell membrane and demonstrate suitable overlap with bacterial protein.

Docking of quinone, NAPQI, NAC, and acetaminophen with hVKOR homology model

Figure 3 shows the superposition of the quinone conformer obtained from the docking analysis with 3KP9 X-ray crystal structure prepared under the experimental crystallography conditions. The figure shows the overlapping between the homology model (cyan) and the model prepared by X-ray crystallography (gray). Figure 3 shows the results of the NAPQI, NAC, and acetaminophen docking with homology-based model of hVKOR.

The ribbon visualization of these molecules is presented in the Figure 4(A–C). The amino acid residues involved in the interaction of the VKOR with these ligands are shown in Figure 4(D–F). Figure 4(A) shows that NAPQI binds to a V-shaped cleft located in the 4-transmembrane bundle. As the 2 D LigPlot diagram for the interacting amino acid residues shows (Figure 4(D)), the ligand was stabilized via interactions with tweleve amino acid residues including; thirteen van der Waals interactions with Ala26, Lys30, Phe55, Gly60, Ser79, Ser81, Leu120, Leu124, Cys135, and Val154. The figure also showed that side chain from Asn80 was involved in

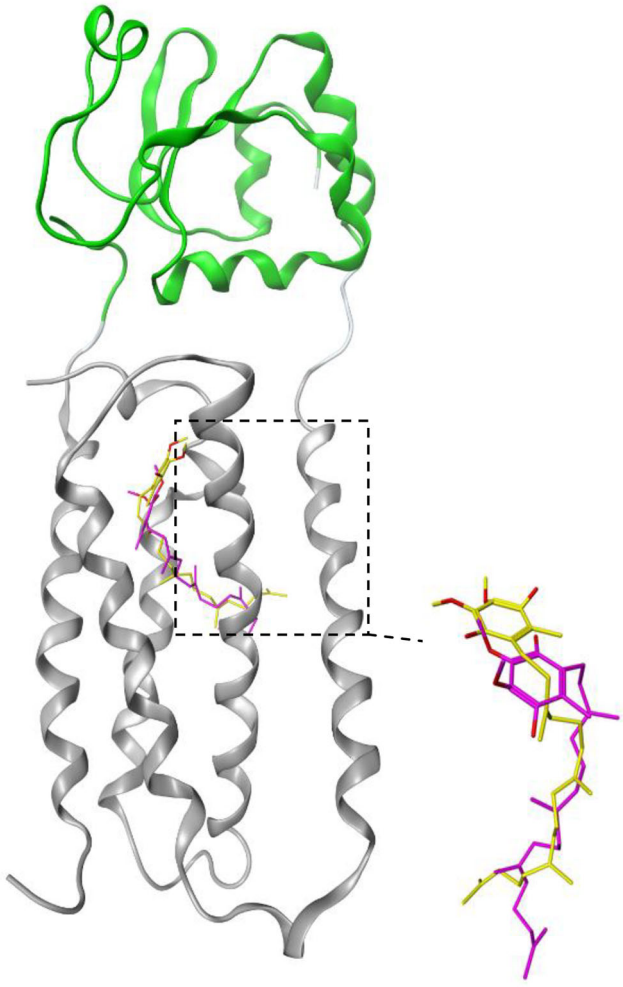

Figure 3. Superposition of the docked conformer of quinone with the bacterial VKOR. The bacterial VKOR and Trx-like domain are shown in gray and green ribbons, respectively. The dotted square contains the quinone binding site. Yellow and magnetic sticks represent the quinone molecules in the x-ray crystal structure of VKOR obtained from experimental crystallography and docking analysis, respectively.

forming a hydrogen bond with oxygen atom from NAPQI. Figure 4(B) shows the interaction of NAC with VKOR, visualized in the ribbon view. The figure shows that NAC binds to the enzyme at close proximity to the site we explained for NAPQI. The visualization of the ligand interaction in 2 D view demonstrated that eight amino acid residues were engaged. The binding was mediated by two hydrogen bonds between hydroxyl moieties of NAC and side chains of Asn80 and Thr138. Furthermore, side chains from six residues involved in van der Waals interactions were including: Ala26, Phe55, Gly60, Ser79, Ser81, and Cys135.

Table 2 compares the amino acid residues involved in the interaction of different ligands with hVKOR. The table shows that from thirteen interacting residues with NAPQI, ten residues were also involved in the NAC binding to VKOR. Figure 4(C) shows the ribbon view of acetaminophen binding site on VKOR. The figure indicates that the ligand attached to the protein in the preplasmatic region, in the vicinity of the terminal part of the TM4 α-helix. The analysis of the amino acids contributed in the acetaminophen interaction with VKOR from LigPlot diagram shows that nine residues shared side chains in the van der Waals interactions. They included: Lys30, Arg33, Ala34, Ser56, Ser57, Arg58, Gly60, Arg61, and Gln78. Table 2 shows that three out of twelve amino acids involved in the acetaminophen binding were identical with those for NAPQI and NAC binding. Figure 4(G) shows the superposition of the binding conformers of the ligands with hVKOR model. There is an overlap between NAPQI and NAC, but not with acetaminophen.

Molecular dynamics simulation of NAPQI, NAC, and acetaminophen with hVKOR homology model

Molecular dynamics (MD) simulation study was performed to address the stability of ligand- protein complexes. RMSD measures the spatial differences between a starting and simulated complex structure and RMSF measures the average displacement of a particle over time from a reference position. RMSF is useful to identify the rigid and flexible regions in protein.

The RMSD and RMSF were calculated between initially docked structure and simulated structure for all protein atoms (Figure 5(A,B)).

All three complexes have overall low RMSD (∼ 0.5 nm). RMSD of the C_α atomic coordinates increases in the beginning up to 2 ns for all three complexes. The plateau after 2 ns indicates that the complex does not fluctuates too much from the reference (Figure 5(A)). However, hVKOR in complex with NAPQI has the lowest RMSD. It confirms the strong binding of the ligand to the protein in agreement with the results of the docking. Figure 5(A) shows that time average of the RMSD of the C_α atoms of hVKOR in complex with all three ligands remains stable. However to investigate the possibility of conformational change in the binding site the RMSD and radius of gyration for the binding site were calculated for each complex (Figure 5(C,D)). As it is clear from this figure the RMSD and radius of gyration for all three ligands in complex with protein is stable indicating the low chance of comformational change in the binding site.The RMSF was calculated by averaging over all atoms of given residues showed in trajectory.

The RMSF curve (Figure 5(B)) shows most of the residues was within the limit of 5 Å, RMSF for NAC and NAPQI were very similar while the one for acetaminophen was higher. It could relate to different binding behavior for acetaminophen-hVKOR complex. Figure 6 shows the residues with the highest fluctuations from RMSF plot for three protein-ligand complexes. The residues with most fluctuation belong to the coils with higher flexibility than other domains of the protein. This figure indicates that the active site residues for NAC and NAPQI complexes are stable with small fluctuations at loops and N and C-terminal region of the protein. Some binding site residues in acetaminophen-hVKOR complex such as Arg33 and Tyr39 have high fluctuations indicating weaker binding of acetaminophen to this site in agreement with the results obtained from the docking. The complexes of NAC and NAPQI with hVKOR show similar deviation and fluctuation validating the consistency of the simulation trajectories.

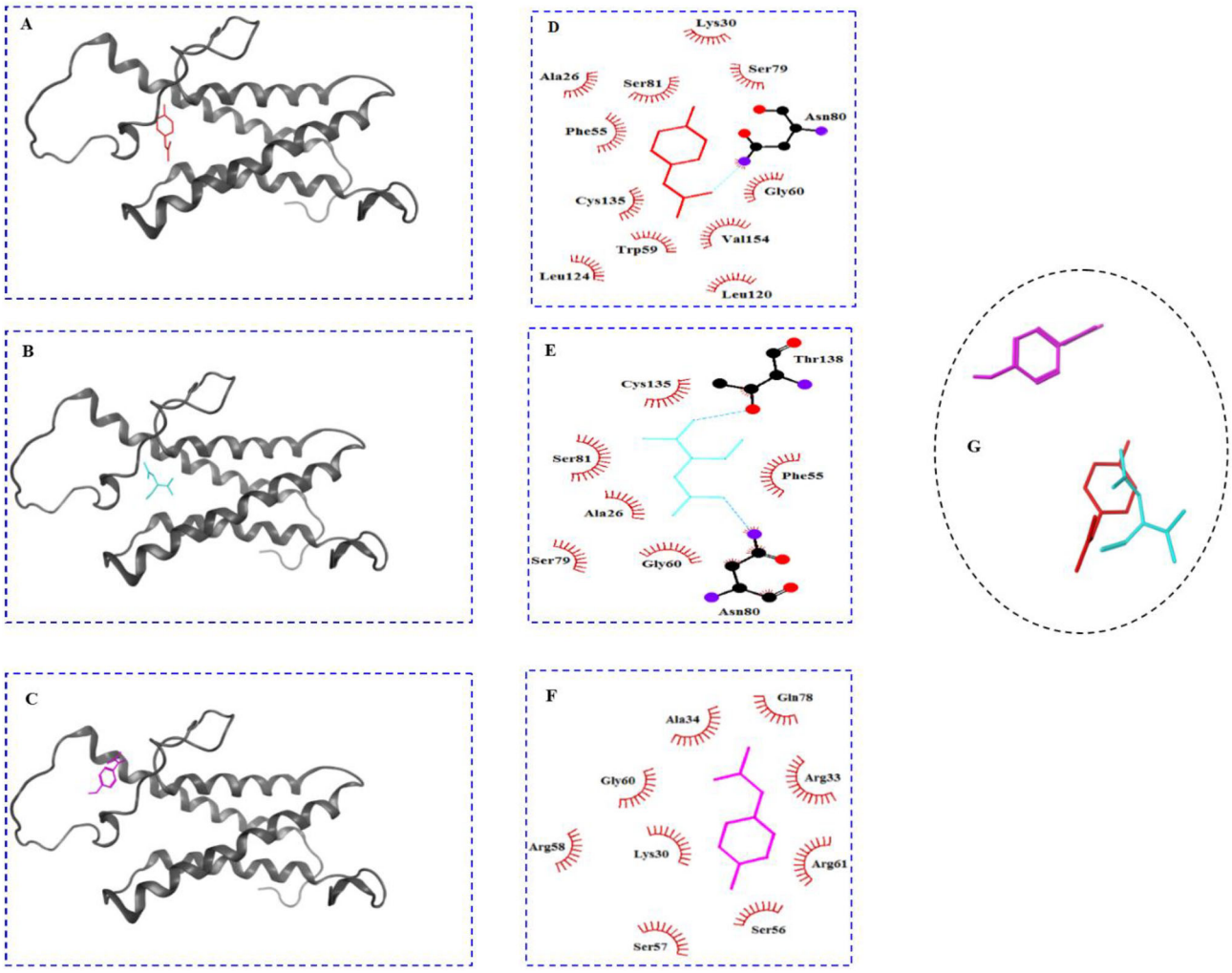

Figure 4. Docking results of the hVKOR homology model with different ligands. The binding site of NAPQI, NAC and acetaminophen in the ribbon view ((A), (B), and (C), respectively), and interacting amino acids diagrams showing the amino acids and chemical bonds involved in the interaction of NAPQI, NAC, and acetaminophen with hVKOR homology model in two dimensional view ((D), (E), and (F), respectively). Superposition of ligands is shown in (G). hVKOR, gray ribbon; NAPQI, red stick; NAC; cyan stick; acetaminophen, magnetic stick, red semi-circle radial spikes: hydrophobic interaction; sky blue dash lines: hydrogen bond.

Table 2. Binding energy and amino acid residues involved in the interaction between different ligands with VKOR.

Ligand	Amino acids involved in non-hydrogen interactions	Amino acids involved in hydrogen bonding	ΔG (kcal/mol)
NAPQI	Ala26, Lys30, Phe55, Gly60, Ser79, Ser81, Leu120, Leu124 Cys135, Val154	Asn80	–6.5
NAC	Ala26, Phe55, Gly60, Ser79, Leu120, Ser81, Cys135	Asn80, *Thr138*	–4.4
Acetaminophen	Lys30, Gly60,*Ser56, , Ala31, Arg33, Ala34, Tyr39, Ser57, Arg58, , Arg61, Gln78*	–	–6.0

NAPQI, N-acetyl-para benzoquinone imine; NAC, N-acetyl cysteine. The bold and the italic styles are representative of the similar and dissimilar amino acids involved in the binding with hVKOR model between NAPQI and NAC or acetaminophen.

The hydrogen bond analysis of hVKOR in complex with NAPQI, NAC and acetaminophen (Figure 7(A)) displayed an average of 102, 103 and 105 hydrogen bonds for each complex, respectively. This figure shows the contacts of residues and ligands are stable during the simulatin. Solvent accessible surface area (SASA) analysis measures the interaction between complexes and solvents. SASA analysis was done for three complexes and the values are plotted in Figure 7(B). We observed that the SASA values for the NAPQI in complex with hVKOR is completely stable during MD simulation in agreement with other results from docking and MD simulation. This figure reveals the average exposure to the solvent area for NAC and acetaminophn remains faily unchanged during the simulation although there are some fluctuations in comparison with NAPQI specially in the plot for acetaminophen. These fluctuations are in agreement with the trend in RMSD and RMSF values could be the result of some minor conformational change in flexible regions of the complex.

Physicochemical and pharmacokinetic characteristics of NAPQI and acetaminophen

Figure 8 shows the comparison of some physicochemical and pharmacokinetic characteristics of NAPQI and acetaminophen. Figure 8(A) shows the bioavailability radars for these

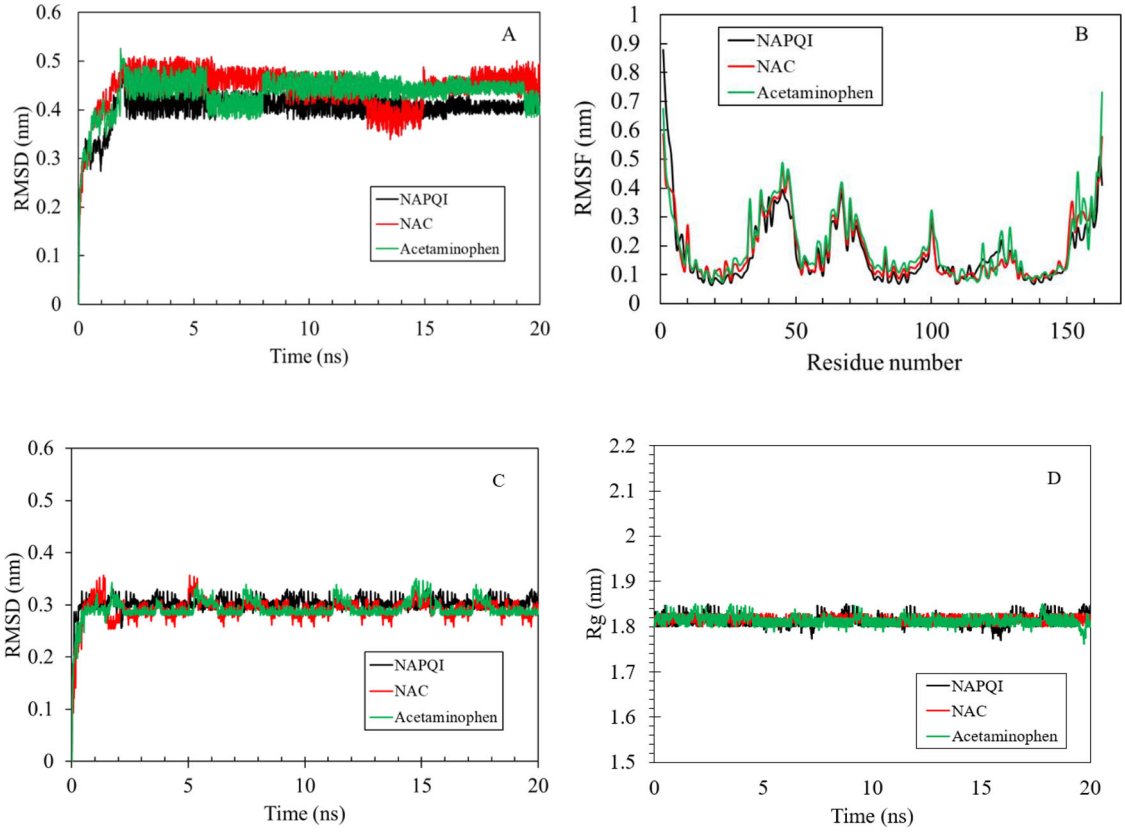

Figure 5. MD simulation results of the hVKOR homology model with three ligands. Root mean square deviation (RMSD) vs time (A), root mean square fluctuation (RMSF) of each residue from hVKOR (B), RMSD of the binding site and radius of gyration (Rg) of the hVKOR binding site (D) from protein ligand complexes. The NAPQI, NAC, and acetaminophen were considered, where the corresponding results are shown in black, red and green lines, respectively.

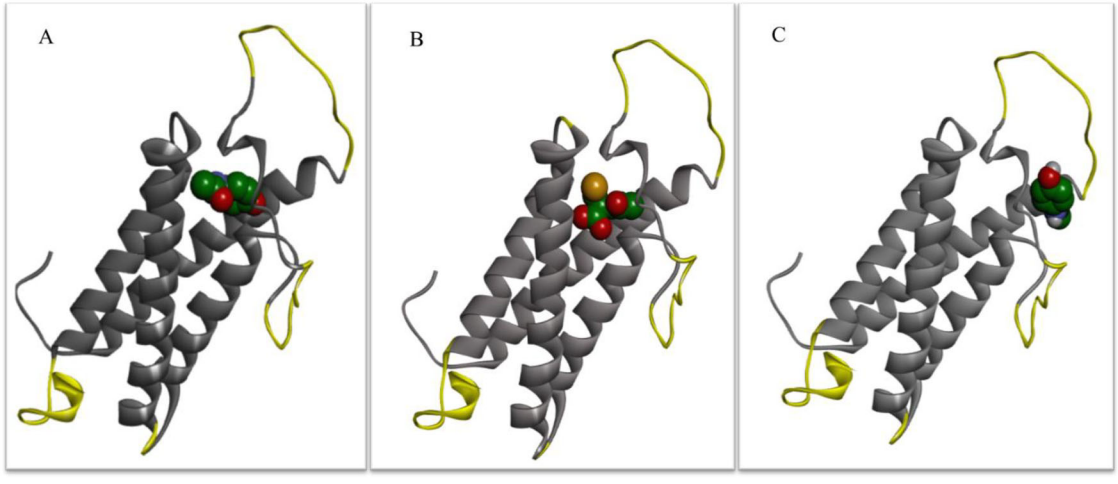

Figure 6. Three-dimensional representation of the regions with the greatest fluctuation during MD simulation of the hVKOR homology model with three ligands. Yellow highlighted regions of the hVKOR with the greatest fluctuations in RMSF plot for (A) NAPQI; (B) NAC; (C) Acetaminophen during 20 ns of MD simulation.

agents. In every radar, six physicochemical descriptors are lipophilicity, size, polarity, solubility, flexibility and saturation. The colored zones are the physicochemical suitable space for oral bioavailability (Daina et al., 2017). The figures indicate that the despite similar molecular size, NAPQI and acetaminophen are different in some descriptors. The water insolubility of acetaminophen is somewhat more than NAPQI. Table 3 shows the amounts of lipophilicity and solubility for NAPQI and acetaminophen. Based on the table, the logarithm of the partition coefficient of NAPQI in a n-octanol/water system (log P), is more than acetaminophen. The water solubility of NAPQI, is about four times more than acetaminophen (26.2 mg/ml compared to 6.94 mg/ml, respectively). Figure 8(C) shows the results of BOILED-Egg plot for NAPQI and acetaminophen. This plot demonstrates an estimation of these molecules permeation into BBB (yellow yolk area), and intestine (white oval area). It shows that both NAPQI and acetaminophen presented in the yellow

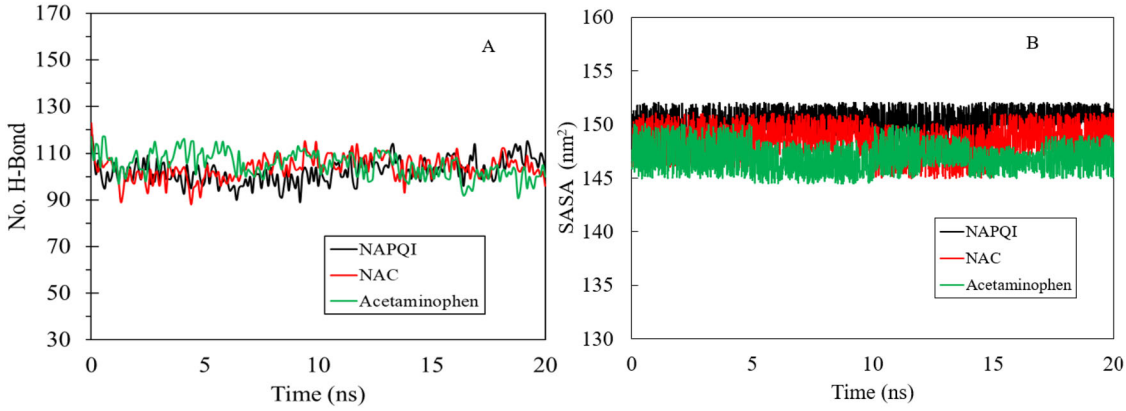

Figure 7. Hydrogen bond analysis (A), solvent accessible surface area of protein ligand complexes (B). NAPQI, NAC, and acetaminophen were considered, where the corresponding results are shown in black, red and green lines, respectively.

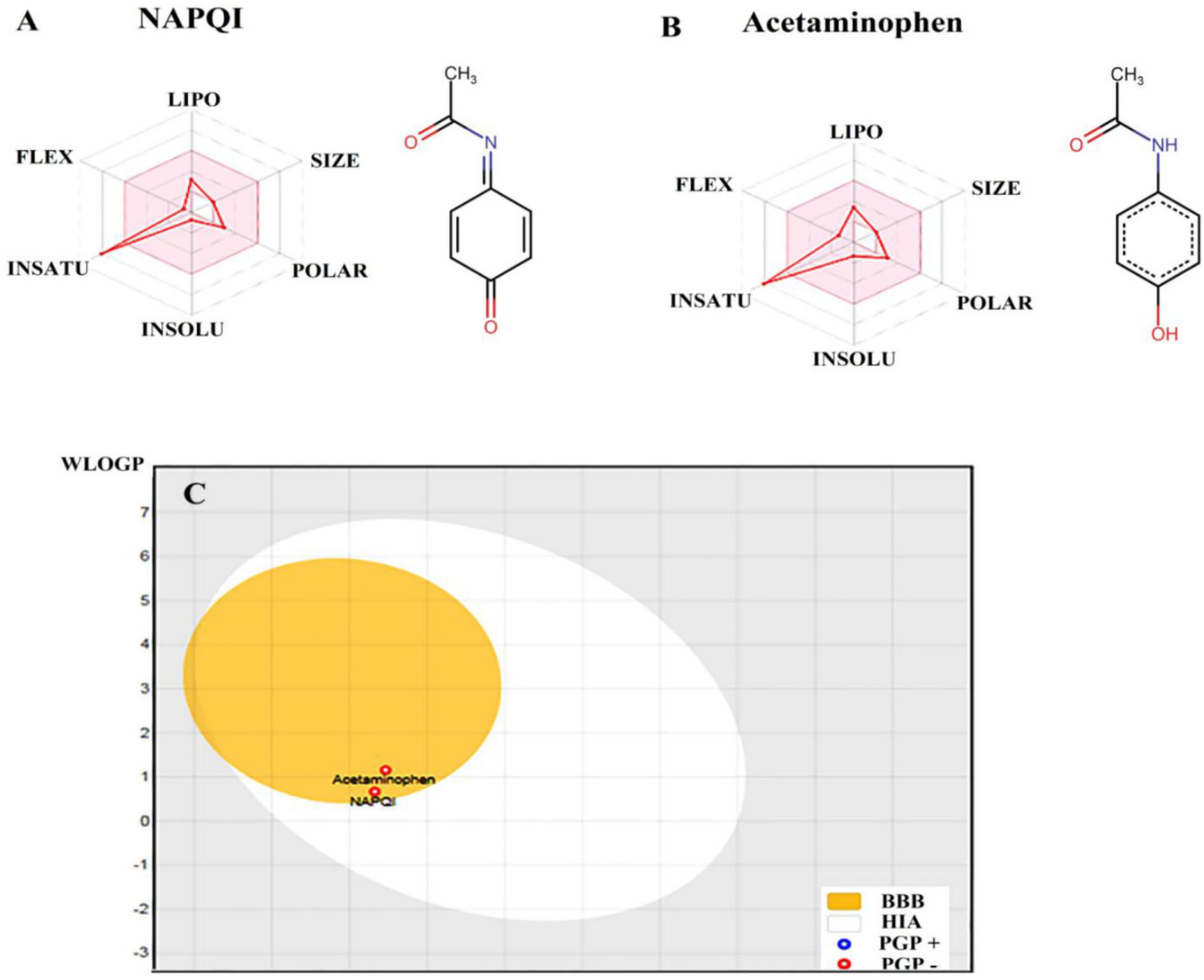

Figure 8. Physicochemical and BBB permeability of NAPQI and acetaminophen. The diagram of physicochemical properties including: lipophilicity, LIPO; molecular size, SIZE; polarity, POLAR; insolubility, INSOLU; instauration, INSATU; molecular flexibility, FLEX, of NAPQI (A) and acetaminophen (B). The BOILED-Egg plot (C), an estimation of NAPQI or acetaminophen permeation into BBB (yellow yolk area), and intestine (white oval area). BBB, blood-brain-barrier; HIA, human intestinal absorption; WLOGP, the log *P* method developed by Wildman and Crippen; TPSA, topological polar surface area; PGP, P-glycoprotein.

Table 3. Physicochemical characteristics of NAPQI and acetaminophen.

	NAPQI[a]	Acetaminophen
Molecular weight (g/mol)	149.15	151.16
Lipophilicity ($LogP_{O/W}$)	1.62	1.21
Water solubility (g/mol)	26.2	6.93

[a]NAPQI, N-acetyl-para benzoquinone imine.

yolk region of the egg-like area in the plot, which is indicative of the possibility of permeation into BBB (Daina & Zoete, 2016). Both molecules are shown by red dots, as PGP^-. This means that none of these molecules were predicted to be effluated by the P-glycoprotein from the central nervous system.

Discussion

Here, the results of the *in silico* analysis predicted the binding sites of acetaminophen, NAPQI, and NAC on hVKOR homology model protein and thereby proposed the molecular details of acetaminophen-induced coagulopathy. In addition, our analysis supports the acetaminophen as the first-line therapy for the fever and pain treatment in patients with COVID-19. However, warns the coagulopathy and cerebral hemorrhage at prolonged applications due to the formation of NAPQI, and is recommended for the monitoring of the coagulation markers such as INR and PT along with the therapy.

Our analysis showed that there was a limited coverage and similarity, and accordingly minimum alignment score between the protein sequences of hVKOR and *Synechococcus sp;* the only species with the available X-ray crystal structure solution for VKOR in PDB (PDB ID: 3KP9) (Li et al., 2010). This made the prokaryotic VKOR inappropriate for using in the docking analysis of the present study. Therefore, the structure of hVKOR was predicted by *in silico* homology modeling, using the ITASSER server (Yang & Zhang, 2015; C. Zhang et al., 2017). Based on the guidelines provided for understanding the results of the ITASSER, normalized Z-score >1 indicates an alignment with high confidence (Yang & Zhang, 2015). The TM-score is a metric for measuring the similarity of two protein structures (Y. Zhang & Skolnick, 2004). The C-score is normally in the range of -5 to 2 and a model of C-score > -1.5 usually has a correct fold, with the TM-score >0.5 (Xu & Zhang, 2010; Yang & Zhang, 2015). Our homology-based model fulfilled these criteria. The homology model used for docking analysis in the present study showed the structure containing a 4-transmembrane (4TM) domain. Based on the Figure 2, the stereochemical parameters of this model agreed favorably with the PDB ID:3KP9, previously reported by Li et al. (2010). Furthermore, the alignment of the homology model with the 3KP9 (prokaryotic (*Synechococcus sp.*) X-ray crystal structure of VKOR showed an RMSD about 1 Å (i.e. 0.96 Å); TM-score, 0.813; and sequence coverage of 0.841, which is indicative of suitable structural homology. In accordance with the template model and the homology models of hVKOR constructed in the previous studies, our model also contained similar secondary structural elements and overall protein folds. The preplasmatic surface of the model comprised a long loop between TM1 and TM2 (Arg35-Ser79). This preplasmatic loop, in accordance with template model, showed all three structural elements, including N-terminal part (called the '1/2-segment'), a short helix (called the '1/2-helix'), and a C-terminal segment. Like the bacterial template contains a highly conserved serine-rich helical segment, Ser52-Ser57. Furthermore, consistent with the homology-constructed model reported by Czogalla *et al.,* the conserved cysteine pairs, Cys43-Cys51 and Cys132-Cys135, in our model are located in the cytoplasmic loop and the fourth trans-membrane α-helix, respectively (Czogalla et al., 2013).

In order to optimize the computational conditioning of the docking analysis, so that, to translate the results to the experimental conditions, at first we extracted the quinone from the X-ray crystal structure of *Synechococcus sp* by Pymol. Then, the binding sites of the molecule under the different docking conditions were compared with its original conformation in 3KP9. The best conditions were selected and applied for all dockings in the present study. This figure beside the Figure 2, indicated the appropriate structural alignment between the homology model and the 3KP9, which are affirmative reason of reliable docking conditions applied here.

Among the residues engaged in the NAPQI binding, Cys135 was reported as a part of the conserved CXXC active site motif, which is present in all VKORs and shares the disulfide bond with Cys132. This cysteine pair plays an important role in the electron transfer pathway and the vitamin K reduction (Li et al., 2010). Consistently, Rost *et al.* have shown that substitution of Cys135 with the serine caused a dramatic decrease in hVKOR activity compared to the wild type (Rost et al., 2005). All published reports have shown a complete loss of VKOR activity if one of the cysteines in the CXXC motif is mutated (Du et al., 2015; Jin et al., 2007; Li et al., 2010; Rost et al., 2005).

Our analysis proposed the involvement of Phe55 and Ser56 in the NAPQI binding to the VKOR. These residues are reported to be the part of a highly conserved serine-rich helical segment (Ser52-Ser57), that beside the endoplasmic reticulum (ER) end of the first transmembrane helix (Leu22–Lys30), and a segment of the fourth transmembrane helix continuing into the large ER loop (Phe131-Thr137), represents putative interaction interfaces for warfarin (Czogalla et al., 2013). Phe55 was indicated to have a pivotal role in vitamin K binding to its binding site on hVKOR (Czogalla et al., 2017). Collectively, our findings support the results of Thijssen *et al.*, which has shown the inhibition of VKOR activity and oxidation of vitamin K by NAPQI in the *in vitro* (Thijssen et al., 2004). We suggest that this was occurring due to two reasons; first, binding of NAPQI to the CXXC motif in VKOR, which interferes with electron transfer from the reducing equivalents to the vitamin K. Second, binding of NAPQI to the Phe55 of Ser52-Ser57 segment that might also hinder the access of the oxidized vitamin K substrate to its binding pocket in the hVKOR active site.

Docking analysis proposed the similar mechanism of the enzyme inhibition by NAC, as that was explained for NAPQI. This is in accordance with the experimental results has been reported, previously (Thijssen et al., 2004). The authors have shown that NAC inhibits the VKOR in a dose-dependent manner; however, its 50% inhibition concentration (IC_{50}) value was more than NAPQI. Our data also showed that the free energy of binding of NAPQI to hVKOR (–6.5 kcal/mol) was more negative than NAC (–4.4 kcal/mol), indicating the strong affinity of NAPQI for enzyme. However, in contrast to NAPQI and NAC bindings, cysteine was not involved in the acetaminophen binding and stabilization. The superposition of the binding poses of NAPQI, NAC and acetaminophen is compatible with our above-mentioned description. It shows NAPQI overlapping with NAC, but not with acetaminophen.

MD simulation was used to consider the RMSD of atomic positions, and RMSF of the backbone atoms of each residue

in hVKOR in binding with three ligands (acetaminophen, NAPQI and NAC). The low variation of RMSD and RMSF values for NAC and NAPQI in interaction with hVKOR clarify that the docked complexes were stable throughout the MD simulation. The lower RMSD for NAPQI reveals stronger binding in the hVKOR binding site and more stability for ligand-protein complex in agreement with docking results. The similarity in RMSF curve for NAC and NAPQI indicated the similar interaction behavior with hVKOR. These results were confirmed by using hydrogen bond analysis and solvent accessible surface area calculations for three ligands in complex with hVKOR. The stability of RMSD and radius of gyration for the binding site of three complexes were another proof of stable binding of the ligands with hVKOR.

To investigate the possibility of cerebral hemorrhage by acetaminophen, we used Swiss ADME server. Then, we calculated the lipophilicity of acetaminophen and NAPQI and also obtained the BBB permeation (BOILED-Egg) plot. Although, the data indicated more lipophilicity of NAPQI than acetaminophen, both of them showed the ability to permeate into the cerebral cell. Previous studies have shown that both acetaminophen and NAC permeate BBB (Björkman, 1995; Katz et al., 2015; van der Marel et al., 2003). But, based on our literature survey, no study has reported about NAPQI detection in CSF or central nervous system (CNS).

Although, the overall balance of harms and benefits of antipyretic treatment of fever in individuals with COVID-19 is unclear, some national and international health services recommend using acetaminophen as the first-line option for fever or pain (CDC, 2020; Team). A recent review of case-control studies suggested that NSAIDs are associated with higher rates of complications after respiratory tract infections, including complicated pneumonia, pleural effusions, prolonged illness, peritonsillar abscess, dissemination of infection to more than one site, or suppuration (Clavé et al., 2019). Up to now, no evidences of those respiratory and cardiovascular adverse effects of NSAIDs in COVID-19 have been reported; but, in a pragmatic and cautionary approach, those drugs were not recommended as the first-line treatment option (Little, 2020). We showed that NAPQI but not acetaminophen was a potential hVKOR inhibitor. NAPQI formation which is believed to be the reason for acetaminophen acute toxicity (Prescott, 1983) has also been reported in the prolonged use of the therapeutic doses, ranging from 2.6 to 6.5 g/d (Bolesta & Haber, 2002). Therefore, despite recognizing the priority of acetaminophen use in comparison to other antipyretics and analgesics in COVID-19, we suppose that the chronic use of acetaminophen in COVID-19 patients may carry the risk of NAPQI formation, VKOR inhibition and consequent hemorrhage. This is compatible with the previous experimental findings that showed the inhibition of vitamin K cycle enzyme activity by NAPQI but not acetaminophen in the washed microsomal preparations (Thijssen et al., 2004). Although, most of the bleeding events and INR increase relating to acetaminophen use have been reported among patients taking anticoagulant therapy, particularly warfarin (Andrews, 2002; Boeijinga et al., 1982; Mahe et al., 2006; Meng et al., 2011; Parra et al., 2007; Rubin et al., 1984), our analysis showed that the binding site of NAPQI on hVKOR is different from that has been previously shown for warfarin. This suggests that anti-coagulopathy effect of NAPQI could be independent of warfarin. These findings are compatible with the previous reported data about the increased INR and PT in acetaminophen overdoses not complicated by hepatic injury (Buckley & Dawson, 1992; Van der Steeg et al., 1995). Therefore, prolonged PT has been suggested as an indicator of the severity of hepatic injury and as an indication of treatment and monitoring in hepatic injury (Makin et al., 1994; Van der Steeg et al., 1995).

Our data suggest the similar mechanism of hVKOR inhibition by NAC and NAPQI, showing the similar binding sites for these molecules on the enzyme. Some evidences have also shown that NAC enhanced the paracetamol effect on the INR (Jepsen & Hansen, 1994), and prolonged the clotting time *in vitro* (Koterba et al., 1995), in patients with adult respiratory distress syndrome (Jepsen et al., 1992), and subsequently in healthy subjects (Jepsen & Hansen, 1994). The potency of NAC to cause coagulopathy in combination with the previously reported data about the NAC concentration in CSF of patients with Parkinson's disease after its oral administration (Katz et al., 2015), warns the enhanced cerebral hemorrhage in COVID-19 patients using NAC.

Our analysis warns the prolonged use of APAP and NAC in COVID-19 patients and suggests the monitoring of INR, PT and PTT while using these drugs. We suggest using alternative medications which some are already practiced for pain management in COVID-19 patients, such as *nonselective NSAIDs* (e.g. ibuprofen, naproxen, and indomethacin) and *Selective COX-2 inhibitors* (e.g. etoricoxib and celecoxib) which are effective for mild-to-moderate pain (El-Tallawy et al., 2020). Furthermore, the opioids could be used for alleviation in COVID-19 patients with moderate-to-severe pain (El-Tallawy et al., 2020).

In conclusion, here our computational analysis provided the detailed molecular mechanism and structural insight into the interaction of acetaminophen, NAPQI, and NAC with hVKOR. We revealed that the complexes of hVKOR with the ligands are stable throughout the simulation. We showed that both NAPQI and NAC, but not acetaminophen, interact with hVKOR, in the same binding site and cause interruption in the vitamin K reduction pathway. Molecular dynamics simulation confirmed the similarity of NAC and NAPQI in interaction with hVKOR. We provided some virtual evidences supporting the anti-coagulopathy effects of the acetaminophen and NAC that have been reported in some clinical, as well as *in vitro* studies. These findings signify the risk of coagulopathy in the chronic use of acetaminophen, particularly among COVID-19 patients, which are susceptible for this harm and prolong prothrombin time. In addition, considering the lipophilicity and BBB permeability of acetaminophen and NAC, our study warns cerebral hemorrhage in COVID-19 and suggests regular PT and INR monitoring in COVID-19 patients taking acetaminophen and/or NAC.

Disclosure statement

The authors claim that there is no conflict of interest.

Funding

This project was supported by the Research Core Grant No. IG-39807 of Tarbiat Modares University.

References

Andrews, F. (2002). Retroperitoneal haematoma after paracetamol increased anticoagulation. *Emergency Medicine Journal*, *19*(1), 84–85. https://doi.org/10.1136/emj.19.1.84

Attouch, H., & Cominetti, R. (1996). A dynamical approach to convex minimization coupling approximation with the steepest descent method. *Journal of Differential Equations*, *128*(2), 519–540. https://doi.org/10.1006/jdeq.1996.0104

Berendsen, H., Van Der Spoel, D., & Van Drunen, R. (1995). GROMACS: A message-passing parallel molecular dynamics implementation. *Computer Physics Communications*, *91*(1-3), 43–56. https://doi.org/10.1016/0010-4655(95)00042-E

Berendsen, H. J. C., Postma, J. P. M., van Gunsteren, W. F., & Hermans, J. (1981). Interaction models for water in relation to protein hydration. In B. Pullman (Ed.), *Intermolecular forces. The Jerusalem symposia on quantum chemistry and biochemistry* (Vol 14). Springer. https://doi.org/10.1007/978-94-015-7658-1_21

Bhardwaj, V. K., Singh, R., Sharma, J., Rajendran, V., Purohit, R., & Kumar, S. (2020). Identification of bioactive molecules from tea plant as SARS-CoV-2 main protease inhibitors. *Journal of Biomolecular Structure and Dynamics*, *38*(1), 1–10. https://doi.org/10.1080/07391102.2020.1766572

Björkman, R. (1995). Central antinociceptive effects of non-steroidal anti-inflammatory drugs and paracetamol. Experimental studies in the rat. *Acta Anaesthesiologica Scandinavica. Supplementum*, *103*, 1–44. https://doi.org/10.1111/j.1399-6576.1995.tb04249.x

Boeijinga, J., Boerstra, E., Ris, P., Breimer, D., & Jeletich-Bastiaanse, A. (1982). Interaction between paracetamol and coumarin anticoagulants. *The Lancet*, *319*(8270), 506. https://doi.org/10.1016/S0140-6736(82)91473-8

Bolesta, S., & Haber, S. L. (2002). Hepatotoxicity associated with chronic acetaminophen administration in patients without risk factors. *Annals of Pharmacotherapy*, *36*(2), 331–333. https://doi.org/10.1345/aph.1A035

Brooks, B. R., Bruccoleri, R. E., Olafson, B. D., States, D. J., Swaminathan, S., & Karplus, M. (1983). CHARMM: A program for macromolecular energy, minimization, and dynamics calculations. *Journal of Computational Chemistry*, *4*(2), 187–217. https://doi.org/10.1002/jcc.540040211

Buckley, N. A., & Dawson, A. H. (1992). Drug interactions with warfarin. *Medical Journal of Australia*, *157*(7), 479–483. https://doi.org/10.5694/j.1326-5377.1992.tb137313.x

CDC. (2020). *2019 novel Coronavirus (2019-nCoV) frequently asked questions and answers*. Centers for Disease Control and Prevention. https://www.cdc.gov/coronavirus/2019-ncov/faq.html

Chen, Z.-M., Fu, J.-F., Shu, Q., Chen, Y.-H., Hua, C.-Z., Li, F.-B., Lin, R., Tang, L.-F., Wang, T.-L., Wang, W., Wang, Y.-S., Xu, W.-Z., Yang, Z.-H., Ye, S., Yuan, T.-M., Zhang, C.-M., & Zhang, Y.-Y. (2020). Diagnosis and treatment recommendations for pediatric respiratory infection caused by the 2019 novel coronavirus. *World Journal of Pediatrics*, *16*(3), 240–247. https://doi.org/10.1007/s12519-020-00345-5

Clavé, S., Rousset-Rouviere, C., Daniel, L., & Tsimaratos, M. (2019). The invisible threat of non-steroidal anti-inflammatory drugs for kidneys. *Frontiers in Pediatrics*, *7*, 520. https://doi.org/10.3389/fped.2019.00520

Czogalla, K. J., Biswas, A., Höning, K., Hornung, V., Liphardt, K., Watzka, M., & Oldenburg, J. (2017). Warfarin and vitamin K compete for binding to Phe55 in human VKOR. *Nature Structural & Molecular Biology*, *24*(1), 77–85. https://doi.org/10.1038/nsmb.3338

Czogalla, K. J., Biswas, A., Wendeln, A.-C., Westhofen, P., Müller, C. R., Watzka, M., & Oldenburg, J. (2013). Human VKORC1 mutations cause variable degrees of 4-hydroxycoumarin resistance and affect putative warfarin binding interfaces. *Blood*, *122*(15), 2743–2750. https://doi.org/10.1182/blood-2013-05-501692

Daina, A., Michielin, O., & Zoete, V. (2017). SwissADME: A free web tool to evaluate pharmacokinetics, drug-likeness and medicinal chemistry friendliness of small molecules. *Scientific Reports*, *7*, 42717. https://doi.org/10.1038/srep42717

Daina, A., & Zoete, V. (2016). A BOILED-Egg to predict gastrointestinal absorption and brain penetration of small molecules. *ChemMedChem*, *11*(11), 1117–1121. https://doi.org/10.1002/cmdc.201600182

de Lima Menezes, G., & da Silva, R. A. (2020). Identification of potential drugs against SARS-CoV-2 non-structural protein 1 (nsp1). *Journal of Biomolecular Structure and Dynamics*, *38*(1), 1–11. https://doi.org/10.1080/07391102.2020.1792992

Du, J.-J., Zhan, C.-Y., Lu, Y., Cui, H.-R., & Wang, X.-Y. (2015). The conservative cysteines in transmembrane domain of AtVKOR/LTO1 are critical for photosynthetic growth and photosystem II activity in Arabidopsis. *Frontiers in Plant Science*, *6*, 238. https://doi.org/10.3389/fpls.2015.00238

El-Tallawy, S. N., Nalamasu, R., Pergolizzi, J. V., & Gharibo, C. (2020). Pain management during the COVID-19 pandemic. *Pain and Therapy*, *9*(2), 453–414. https://doi.org/10.1007/s40122-020-001904

Essmann, U., Perera, L., Berkowitz, M. L., Darden, T., Lee, H., & Pedersen, L. G. (1995). A smooth particle mesh Ewald method. *The Journal of Chemical Physics*, *103*, 8577–8593. https://doi.org/10.1063/1.470117

Gupta, R., & Misra, A. (2020). Contentious issues and evolving concepts in the clinical presentation and management of patients with COVID-19 infectionwith reference to use of therapeutic and other drugs used in co-morbid diseases (Hypertension, diabetes etc). *Diabetes & Metabolic Syndrome. Diabetes & Metabolic Syndrome*, 14(3), 251–254. https://doi.org/10.1016/j.dsx.2020.03.012

Hashemi, S. A., Bathaie, S. Z., & Mohagheghi, M.-A. (2020a). Interaction of saffron carotenoids with catalase: *In vitro, in vivo* and molecular docking studies. *Journal of Biomolecular Structure & Dynamics*, *38*(13), 3916–3911. https://doi.org/10.1080/07391102.2019.1668302

Hashemi, S. A., Bathaie, S. Z., & Mohagheghi, M. A. (2020b). Crocetin and crocin decreased cholesterol and triglyceride content of both breast cancer tumors and cell lines. *Avicenna Journal of Phytomedicine*, *10*(4), 384–397.

Hashemi, S. A., Karami, M., & Bathaie, S. Z. (2020). Saffron carotenoids change the superoxide dismutase activity in breast cancer: In vitro, in vivo and in silico studies. *International Journal of Biological Macromolecules*, *158*, 845–853. https://doi.org/10.1016/j.ijbiomac.2020.04.063

Huang, J., & Mackerell, A. D. (2013). CHARMM36 all-atom additive protein force field: Validation based on comparison to NMR data. *Journal of Computational Chemistry*, *34*(25), 2135–2145. https://doi.org/10.1002/jcc.23354

Jepsen, S., & Hansen, A. (1994). The influence of N-acetylcysteine on the measurement of prothrombin time and activated partial thromboplastin time in healthy subjects. *Scandinavian Journal of Clinical and Laboratory Investigation*, *54*(7), 543–547. https://doi.org/10.3109/00365519409088566

Jepsen, S., Herlevsen, P., Knudsen, P., Bud, M. I., & Klausen, N. (1992). Antioxidant treatment with N-acetylcysteine during adult respiratory distress syndrome: A prospective, randomized, placebo-controlled study. *Critical Care Medicine*, *20*(7), 918–923. https://doi.org/10.1097/00003246-199207000-00004

Jin, D.-Y., Tie, J.-K., & Stafford, D. W. (2007). The conversion of vitamin K epoxide to vitamin K quinone and vitamin K quinone to vitamin K hydroquinone uses the same active site cysteines. *Biochemistry*, *46*(24), 7279–7283. https://doi.org/10.1021/bi700527j

Katz, M., Won, S. J., Park, Y., Orr, A., Jones, D. P., Swanson, R. A., & Glass, G. A. (2015). Cerebrospinal fluid concentrations of N-acetylcysteine after oral administration in Parkinson's disease. *Parkinsonism & Related Disorders*, *21*(5), 500–503. https://doi.org/10.1016/j.parkreldis.2015.02.020

Koterba, A. P., Smolen, S., Joseph, A., Basista, M. H., & Brecher, A. S. (1995). Coagulation protein function. II. Influence of thiols upon

acetaldehyde effects. *Alcohol (Fayetteville, N.Y.)*, *12*(1), 49–57. https://doi.org/10.1016/0741-8329(94)00069-P

Kouhpayeh, S., Shariati, L., Boshtam, M., Rahimmanesh, I., Mirian, M., Zeinalian, M., Salari-Jazi, A., Khanahmad, N., Damavandi, M. S., Sadeghi, P., & Khanahma, H. (2020). The molecular story of COVID-19; NAD + depletion addresses all questions in this infection. *Preprints,* 2020030346. https://doi.org/10.20944/preprints202003.0346.v1

Li, W., Schulman, S., Dutton, R. J., Boyd, D., Beckwith, J., & Rapoport, T. A. (2010). Structure of a bacterial homologue of vitamin K epoxide reductase. *Nature*, *463*(7280), 507–512. https://doi.org/10.1038/nature08720

Lippi, G., Plebani, M., & Henry, B. M. (2020). Thrombocytopenia is associated with severe coronavirus disease 2019 (COVID-19) infections: A meta-analysis. *Clinica Chimica Acta; International Journal of Clinical Chemistry*, *506*, 145–148. https://doi.org/10.1016/j.cca.2020.03.022

Little, P. (2020). *Non-steroidal anti-inflammatory drugs and COVID-19*. British Medical Journal Publishing Group, *368*, m1185. https://doi.org/10.1136/bmj.m1185

Liu, J., Liu, Y., Xiang, P., Pu, L., Xiong, H., Li, C., Zhang, M., Tan, J., Xu, Y., Song, R., Song, M., Wang, L., Zhang, W., Han, B., Yang, L., Wang, X., Zhou, G., Zhang, T., … Song, R. (2020). Neutrophil-to-lymphocyte ratio predicts severe illness patients with 2019 Novel Coronavirus in the early stage. *Journal of Translational Medicine*, *18*(206), 1–12. https://doi.org/10.1186/s12967-020-02374-0

Mackerell, A. D., Bashford, D., Bellott, M., Dunbrack, R. L., Evanseck, J. D., Field, M. J., Fischer, S., Gao, J., Guo, H., Ha, S., Joseph-Mccarthy, D., Kuchnir, L., Kuczera, K., Lau, F. T. K., Mattos, C., Michnick, S., Ngo, T., Nguyen, … Karplus, M. (1998). All-Atom Empirical Potential for Molecular Modeling and Dynamics Studies of Proteins. *The Journal of Physical Chemistry. B,* 102(18), 3586–3616. https://doi.org/10.1021/jp973084f

Mahe, I., Bertrand, N., Drouet, L., Bal Dit Sollier, C., Simoneau, G., Mazoyer, E., Caulin, C., & Bergmann, J. F. (2006). Interaction between paracetamol and warfarin in patients: A double-blind, placebo-controlled, randomized study. *Haematologica*, *91*(12), 1621–1627. https://doi.org/10.3324/%25x

Mahmud, S., Uddin, M. A. R., Zaman, M., Sujon, K. M., Rahman, M. E., Shehab, M. N., Islam, A., Alom, W., Amin, A., Akash, A. S. H., & AbuSaleh, M. A. (2020). Molecular docking and dynamics study of natural compound for potential inhibition of main protease of SARS-CoV-2. *Journal of Biomolecular Structure and Dynamics*, *38*(1), 1–9. https://doi.org/10.1080/07391102.2020.1796808

Makin, A., Wendon, J., & Williams, R. (1994). Management of severe cases of paracetamol overdosage. *British Journal of Hospital Medicine*, *52*(5), 210–213.

Meng, X.-Y., Zhang, H.-X., Mezei, M., & Cui, M. (2011). Molecular docking: A powerful approach for structure-based drug discovery. *Current Computer-Aided Drug Design*, *7*(2), 146–157. https://doi.org/10.2174/157340911795677602

Noah Berland, M., Andrea Greene, M., Suvam Neupane, M., Julian Watson, M., Robert Allen, M., & Dilip, M. (2020). COVID-19 in the emergency department. *Cough*, *72*, 65.67–78.62.

Nouri, A., Heidarian, E., & Nikoukar, M. (2017). Effects of N-acetyl cysteine on oxidative stress and TNF-α gene expression in diclofenac-induced hepatotoxicity in rats. *Toxicology Mechanisms and Methods*, *27*(8), 561–567. https://doi.org/10.1080/15376516.2017.1334732

Parra, D., Beckey, N. P., & Stevens, G. R. (2007). The effect of acetaminophen on the international normalized ratio in patients stabilized on warfarin therapy. *Pharmacotherapy*, *27*(5), 675–683. https://doi.org/10.1592/phco.27.5.675

Poole, L. B. (2015). The basics of thiols and cysteines in redox biology and chemistry. *Free Radical Biology & Medicine*, *80*, 148–157. https://doi.org/10.1016/j.freeradbiomed.2014.11.013

Prescott, L. (1983). Paracetamol overdosage. Pharmacological considerations and clinical management. *Drugs*, *25*(3), 290–314. https://doi.org/10.2165/00003495-198325030-00002

Rost, S., Fregin, A., Hünerberg, M., Bevans, C. G., Müller, C. R., & Oldenburg, J. (2005). Site-directed mutagenesis of coumarin-type anticoagulant-sensitive VKORC1: Evidence that highly conserved amino acids define structural requirements for enzymatic activity and inhibition by warfarin. *Thrombosis and Haemostasis*, *94*(4), 780–786. https://doi.org/10.1160/TH05-02-0082

Rout, J., Swain, B. C., & Tripathy, U. (2020). In silico investigation of spice molecules as potent inhibitor of SARS-CoV-2. *Journal of Biomolecular Structure and Dynamics*, *38*(1), 1–15. https://doi.org/10.1080/07391102.2020.1819879

Rubin, R., Mentzer, R., & Budzynski, A. (1984). Potentiation of anticoagulant effect of warfarin by acetaminophen (Tylenol). In U. W. Christians (Eds.), *Clinical research* (Vol. 32, No. 3, pp. A698-A698). Slack Inc.

Salehi, S., Abedi, A., Balakrishnan, S., & Gholamrezanezhad, A. (2020). Coronavirus disease 2019 (COVID-19): A systematic review of imaging findings in 919 patients. *AJR: American Journal of Roentgenology*, *215*(1), 87–87. https://doi.org/10.2214/AJR.20.23034

Shadnia, S., Dasgar, M., Taghikhani, S., Mohammadirad, A., Khorasani, R., & Abdollahi, M. (2007). Protective effects of alpha-tocopherol and N-acetyl-cysteine on diazinon-induced oxidative stress and acetylcholinesterase inhibition in rats. *Toxicology Mechanisms and Methods*, *17*(2), 109–115. https://doi.org/10.1080/15376510600860318

Shalby, A. B., Assaf, N., & Ahmed, H. H. (2011). Possible mechanisms for N-acetyl cysteine and taurine in ameliorating acute renal failure induced by cisplatin in rats. *Toxicology Mechanisms and Methods*, *21*(7), 538–546. https://doi.org/10.3109/15376516.2011.568985

Song, Y., Liu, P., Shi, X. L., Chu, Y. L., Zhang, J., Xia, J., Gao, X. Z., Qu, T., & Wang, M. Y. (2020). SARS-CoV-2 induced diarrhoea as onset symptom in patient with COVID-19. *Gut*, *69*(6), 1143–1144. http://dx.doi.org/10.1136/gutjnl-2020-320891

Tang, N., Li, D., Wang, X., & Sun, Z. (2020). Abnormal coagulation parameters are associated with poor prognosis in patients with novel coronavirus pneumonia. *Journal of Thrombosis and Haemostasis*, *18*(4), 844–847. https://doi.org/10.1111/jth.14768

Team, D. (2020). EMA advice on the use of NSAIDs for Covid-19, 58, No 5. https://doi.org/10.1136/dtb.2020.000021

Thijssen, H. H., Soute, B. A., Vervoort, L. M., & Claessens, J. G. (2004). Paracetamol (acetaminophen) warfarin interaction: NAPQI, the toxic metabolite of paracetamol, is an inhibitor of enzymes in the vitamin K cycle. *Thrombosis and Haemostasis*, *92*(4), 797–802. https://doi.org/10.1160/TH04-02-0109

Trott, O., & Olson, A. J. (2010). AutoDock Vina: Improving the speed and accuracy of docking with a new scoring function, efficient optimization, and multithreading. *Journal of Computational Chemistry*, *31*(2), 455–461. https://doi.org/10.1002/jcc.21334

van der Marel, C. D., Anderson, B. J., Pluim, M. A. L., de Jong, T. H. R., Gonzalez, A., & Tibboel, D. (2003). Acetaminophen in cerebrospinal fluid in children. *European Journal of Clinical Pharmacology*, *59*(4), 297–302. https://doi.org/10.1007/s00228-003-0622-2

Van Der Spoel, D., Lindahl, E., Hess, B., Groenhof, G., Mark, A. E., & Berendsen, H. J. C. (2005). GROMACS: Fast, flexible, and free. *Journal of Computational Chemistry*, *26*(16), 1701–1718. https://doi.org/10.1002/jcc.20291

Van der Steeg, J., DiSanto, S., & Abendroth, T. (1995). The effect of acetaminophen on the prothrombin time assay. *Journal of Toxicology, Clinical Toxicology*, *33*, 512.

Wang, D., Hu, B., Hu, C., Zhu, F., Liu, X., Zhang, J., Wang, B., Xiang, H., Cheng, Z., Xiong, Y., Zhao, Y., Li, Y., Wang, X., & Peng, Z. (2020). Clinical characteristics of 138 hospitalized patients with 2019 novel coronavirus–infected pneumonia in Wuhan, China. *JAMA*, *323*(11), 1061. http://doi:10.1001/jama.2020.1585

Xu, J., & Zhang, Y. (2010). How significant is a protein structure similarity with TM-score = 0.5? *Bioinformatics*, *26*(7), 889–895. https://doi.org/10.1093/bioinformatics/btq066

Yang, J., & Zhang, Y. (2015). I-TASSER server: New development for protein structure and function predictions. *Nucleic Acids Research*, *43*(W1), W174–W181. https://doi.org/10.1093/nar/gkv342

Zhang, C., Freddolino, P. L., & Zhang, Y. (2017). COFACTOR: Improved protein function prediction by combining structure, sequence and protein-protein interaction information. *Nucleic Acids Research*, *45*(W1), W291–W299. https://doi.org/10.1093/nar/gkx366

Zhang, Y., & Skolnick, J. (2004). Scoring function for automated assessment of protein structure template quality. *Proteins*, *57*(4), 702–710. https://doi.org/10.1002/prot.20264